Measuring temperature profiles in high-power optical fiber components

Vladimir Goloborodko, Shay Keren, Amir Rosenthal, Boris Levit, and Moshe Horowitz

We demonstrate a new method for measuring changes in temperature distribution caused by coupling a high-power laser beam into an optical fiber and by splicing two fibers. The measurement technique is based on interrogating a fiber Bragg grating by using low-coherence spectral interferometry. A large temperature change is found owing to coupling of a high-power laser into a multimode fiber and to splicing of two multimode fibers. Measurement of the temperature profile rather than the average temperature along the grating allows study of the cause of fiber heating. The new measurement technique enables us to monitor in real time the temperature profile in a fiber without the affecting system operation, and it might be important for developing and improving the reliability of high-power fiber components. © 2003 Optical Society of America

OCIS codes: 060.2370, 060.2300, 050.2770.

1. Introduction

During past years there has been a growing interest in developing high-power fiber components and sources. Recently a fiber laser with an end pumping that generates as much as 110 W of average power has been demonstrated.[1] A theoretical study indicated that thermal, stress, and thermo-optics effects may play a significant role in high-power lasers.[2] Moreover fiber imperfections such as optical defects at the fiber end may practically limit the maximum power of the optical components. Therefore there is a need to control and monitor the temperature of high-power fiber components at critical points in the system in order to maintain the performance and avoid damage to components.

Fiber Bragg grating sensors are widely used for measuring strain, pressure, and temperature.[3] In most research the whole grating is considered a single sensor, and therefore the measurement result gives the average temperature or stress along the whole grating. Since a fiber grating is a distributed element it is possible to measure the spatial distribution of the temperature or the stress along the grating. The complex transfer function of a grating can be measured with a tunable laser[4] or a low-coherence spectral interferometry technique.[5] The structure of the grating can be calculated from the complex transfer function by using the Fourier transform[4] or the Gabor transform.[5] Since the temperature or stress affects the grating structure, the profile of the temperature or stress along the grating can be calculated from the measured grating parameters. In this research we experimentally study temperature distribution in a fiber caused by coupling a high-power laser beam into a fiber and by splicing two multimode fibers. Writing a Bragg grating into the fiber allows the temperature to be measured. The Bragg wavelength of the grating is different from the wavelength of the high-power laser. Therefore the measurement can be performed in real time without affecting operation of the fiber system. A large temperature increase was measured when an argon-ion laser beam was coupled into the fiber and when two fibers were spliced together. Measurement of the temperature profile rather than measurement of the average temperature allows study of the cause of fiber heating.

2. Experimental Scheme

A schematic description of our experimental setup for measuring the temperature change in a fiber is shown in Fig. 1. Figure 1(a) shows the setup for measuring the temperature distribution caused by coupling a high-power laser into an optical fiber. A uniform fiber Bragg grating was written at the end of
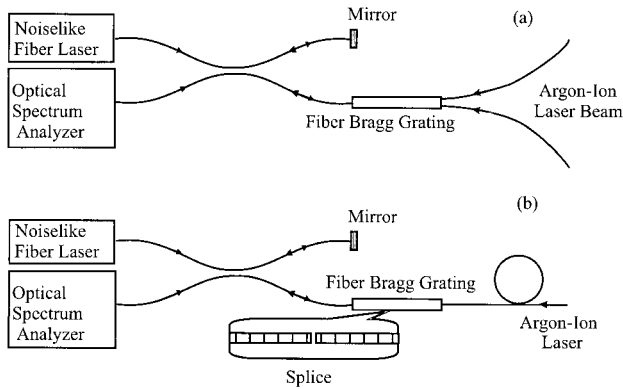
Fig. 1. Schematic description of the experimental setup used to measure the temperature profile caused (a) by coupling a high-power argon-ion laser beam into a fiber and (b) by splicing two optical fibers.

the fiber to measure the temperature profile. The maximum reflection coefficient of the grating was ~50%. The grating was written in a hydrogen-loaded optical fiber by illuminating the fiber with a UV laser beam via a phase mask. After the grating was written, the fiber was cleaved at the location where the grating was written and was placed inside a metallic holder. After the fiber was cleaved, the length of the grating was ~0.6 cm and the maximum reflection coefficient reduced to ~7%. The high-power light source that was coupled into the fiber was an argon-ion laser with power of 1–6 W that operated in a multiline mode in the wavelength regime $\lambda =$ 458–514 nm. The argon-ion beam was coupled through the grating. However, since the central wavelength of the grating was 1542 nm, the grating did not reflect the argon-ion beam and the measurement could be performed in real time without affecting the coupling. The temperature variation caused by coupling the argon-ion laser affected the spatial distribution of the grating parameters. The parameters of the grating were interrogated by using low-coherence spectral interferometry.[5] The low-coherence light source was a broadband fiber laser that operated in the noiselike mode of operation[6,7] and generated pulses with a spectral width of ~70 nm, an average power of 40 mW, a pulse duration of ~2 ns, and a central wavelength of ~1560 nm. The interference spectrum of a light beam reflected from the grating and a light beam reflected from a reference mirror was measured with an optical spectrum analyzer. The interference spectrum was used to obtain the parameters of the grating and the temperature profile as described below. The fiber used in our experiments (bare Corning SMF-28 fiber with a core diameter of 8.2 μm and a cladding diameter of 125 μm) supports only a single propagation mode at the wavelength used to interrogate the grating. However, the fiber becomes a multimode fiber at the wavelength of the high-power argon-ion laser.

Figure 1(b) shows the setup for measuring the temperature distribution around a region where two fi-

bers where spliced together. In our experiment the fiber was cleaved and spliced. Then a grating with a length of ~20 mm and a central wavelength of 1542 nm was written at the splice region of the fiber by using a uniformly distributed phase mask. The high-power laser was an argon-ion laser that was coupled into the fiber. The splice region was located at a distance of ~20 cm from the fiber end, and therefore the temperature change due to coupling of the argon-ion laser did not significantly affect temperature measurement at the splice region.

The grating structure was interrogated with a low-coherence spectral interferometry method as described above. Owing to fiber deformation induced by the splicing, the grating parameters were not spatially uniform even before the argon-ion laser was turned on. However, we could measure the temperature change by comparing the grating structure before and after the argon-ion laser was turned on.

3. Result Analysis

Fiber Bragg gratings are formed by a permanent periodic perturbation of the refractive index of the fiber that can be described as[8]

$$n(z) = n_0(z) + n_1(z)\cos\left[\frac{2\pi}{\Lambda}z + \theta(z)\right], \quad (1)$$

where $n_0(z)$ is the average refractive-index change, $n_1(z)$ is the amplitude of the refractive-index modulation, Λ is the periodicity of the grating, and $\theta(z)$ is the chirp parameter that describes spatial changes in the grating periodicity. Since a fiber Bragg grating is a linear component, it can be characterized by its impulse response $h(t)$. A temperature variation along the grating changes the average refractive index $\delta n_0(z)$ and the periodicity of the grating $\delta\theta(z)$. Therefore a variation in the temperature changes the local Bragg wavelength λ_B along the grating. The dependence of the local Bragg wavelength shift on the change in the average refractive index and the chirp parameter is given by

$$\delta\lambda_B(z) = 2\Lambda\delta n_0(z) - \frac{\Lambda^2 n_{avg}}{\pi}\frac{d[\delta\theta(z)]}{dz}, \quad (2)$$

where n_{avg} is the average refractive index along the whole grating. The first term in Eq. (2) is caused by the temperature dependence of the refractive index, while the second term is caused by thermal expansion of the fiber material.

The connection between the local Bragg wavelength shift and the temperature change δT at a wavelength $\lambda = 1.5$ μm, of a silica fiber is given by[3]

$$\frac{1}{\lambda_B}\frac{\delta\lambda_B}{\delta T} = 6.67 \times 10^{-6} \text{ °C}^{-1}. \quad (3)$$

Therefore the spatial temperature profile along the grating can be directly obtained from the spatial distribution of the Bragg wavelength along the grating. The measurement results of the interference spec-

trum can be analyzed with the Fourier or the Gabor transform. A Fourier transform performed on the measured interference spectrum gives the impulse response of the grating.[5] In general, the structure of a grating can be found from its impulse response by using a relatively complex algorithm based on the inverse-scattering theory.[9] However, when the reflection of the grating is weak the spatial distribution of the grating can be directly obtained from its impulse response by using the first-order Born approximation.[4] A comparison of the first-order Born approximation with results of a numerical simulation shows that the Born approximation becomes accurate in a uniformly distributed grating when the maximum reflectivity of the grating is lower than ~30%. In gratings with a stronger reflection coefficient the Born approximation can be used to analyze the region at the beginning of the grating where the reflection has not yet become strong enough.

When the first-order Born approximation is used, the impulse response of the grating equals[10]

$$h(z) = \kappa(z)\exp[i\phi(z)], \qquad (4)$$

where $\kappa(z) = \pi n_1(z) = \lambda$ is the complex coupling coefficient and

$$\phi(z) = 4\pi/\lambda \int_0^z n_0(z')\mathrm{d}z' - \theta(z)$$

is the accumulated longitudinal phase. The connection between the shift in the local Bragg wavelength and the change in the accumulate phase $\delta\phi(z)$ is given by

$$\delta\lambda_B(z) = -\frac{\mathrm{d}[\delta\phi(z)]}{\mathrm{d}z}\lambda_B\Lambda. \qquad (5)$$

The spatial distribution of the local Bragg wavelength of the grating can be calculated from the impulse response by using Eqs. (4) and (5). Then the temperature distribution along the grating can be obtained from the profile of the local Bragg wavelength by using Eq. (3).

Another approach for calculating the distribution of the local Bragg wavelength along a weakly reflecting grating is based on use of the combined time-frequency Gabor transform.[11] The Gabor transform enables the profile of the local Bragg wavelength along the grating to be obtained directly without the need to calculate the grating parameters.

The Gabor transform of a spectrum $I(\omega)$ is defined as

$$G(t, \Omega) = \int_{-\infty}^{\infty} I(\omega)W(\omega - \Omega)\exp(-i\omega t)\mathrm{d}\omega, \qquad (6)$$

where $W(\omega - \Omega)$ is a window function centered around a frequency $\omega = \Omega$. The result of the Gabor transform of the measured interference spectrum gives the time response of the grating for pulses cen-

tered around the frequency Ω.[5] The average reflection wavelength at time t, $\overline{\lambda_B}(t)$, is given by

$$\overline{\lambda_B}(t) = \frac{\int_{-\infty}^{\infty} \lambda|G(t, \lambda)|\mathrm{d}\lambda}{\int_{-\infty}^{\infty} |G(t, \lambda)|\mathrm{d}\lambda}. \qquad (7)$$

When the grating is weak the spectrum of the wave reflected from a specific location of the grating is centered around the local Bragg wavelength of the region. Therefore, when the reflection coefficient of the grating is small enough ($R \leq 50\%$), the average reflection wavelength at time t, $\overline{\lambda_B}(t)$ approximately equals the local Bragg grating of the grating at location $z = tc = 2n_{\mathrm{avg}}$, where c is the light velocity and $z = 0$ is the location where the grating starts. The shift in the local Bragg wavelength due to the temperature change along the fiber can be calculated by subtracting the local Bragg wavelength before and after the argon-ion laser was turned on.

As explained below the Fourier analysis gives a better spatial resolution than the Gabor analysis. However, the results of the Gabor analysis are less affected by measurement noise, and therefore the Gabor analysis gave better and more stable results in our experiments. We checked the accuracy of our analysis by calculating theoretically the change in the impulse response of a grating due to a given temperature profile along the fiber. By comparing the results of Gabor and the Fourier analysis with the given temperature profile, we found that the Gabor transform enables an accurate analysis of gratings with a stronger reflection coefficient than can be analyzed by using a Fourier transform. When the Gabor transform was used, uniform gratings with a reflection coefficient as high as 50% could be accurately analyzed, while the maximum reflection coefficient of the uniform gratings that could be accurately analyzed by using Fourier transform was only ~30%.

The spatial resolution of our measurement is determined by the minimum between the bandwidths of the laser and the grating. Assuming a Gaussian spectrum with a full width at half-maximum $\Delta\lambda$, the temporal resolution of the impulse response equals

$$\delta t = \frac{4 \ln(2)\lambda^2}{\pi c \Delta\lambda}. \qquad (8)$$

Assuming that the reflection coefficient of the Gaussian grating is smaller than ~30%, the spatial resolution of the measurement equals $\delta z = c\delta t/2n_{\mathrm{avg}}$. For a light source with a bandwidth of 70 nm the spatial resolution can be as short as $\delta z \simeq 10$ μm.[5] When the Gabor transform is used, the bandwidth is limited by the width of the Gabor window. When a window with a bandwidth of 1 nm is used, the spatial resolution reduces to ~0.7 mm. The use of the Gabor transform limits the spatial resolution of the mea-
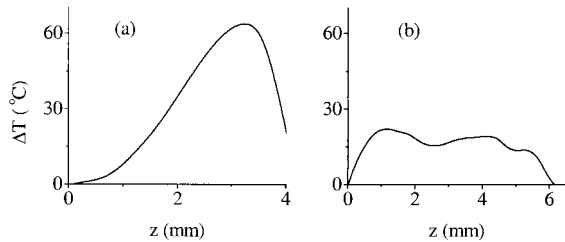
Fig. 2. Two typical temperature profiles measured in a steady-state condition when an argon-ion laser with a power of 3 W was coupled into a fiber. The results are analyzed by using the Gabor transform.

surement. However, the reduced resolution and the low-pass filtering operation involved in calculating the Gabor transform and the average wavelength significantly reduce the effect of the noise in the results. Therefore we found that the Gabor transform gave a more repeatable and smoother result when we analyzed the result of our experiments.

The theoretical resolution of the temperature measurement is limited by the resolution of our spectrum analyzer. When a spectrum analyzer with a resolution $\delta\lambda = 0.015$ nm is used, the minimal temperature resolution, calculated with Eq. (3) equals $\delta T \simeq 1.45$ °C. In practice the resolution in our measurement was limited by the noise added to the measurements. In our experiments the noise in the temperature measurement was ~3 °C, and we could not observe a temperature change below this noise.

4. Experimental Results

A. Temperature Change Caused by Coupling a High-Power Laser Beam into an Optical Fiber

The experimental results obtained when a high-power argon-ion laser was coupled into a fiber are shown in Figs. 2 and 3. When the argon-ion laser was turned on, we measured large temperature fluctuations for several minutes. After ~20 min a steady-state temperature profile was obtained when the fiber end was thermally isolated. When the Gabor transform was used, the amplitude of the temporal fluctuation of the measured temperature was only ~3 °C before the argon-ion laser was turned on.
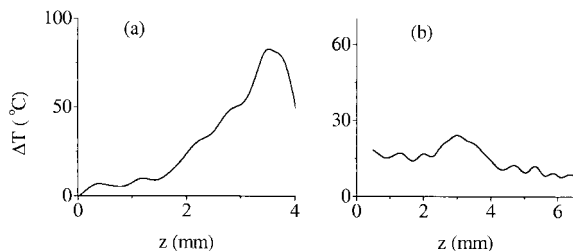
Fig. 3. Two typical temperature profiles measured in a steady-state condition when an argon-ion laser with a power of 3 W was coupled into a fiber. The results are analyzed by using the Fourier transform.

When the argon-ion laser was turned on for ~20 min, the temporal fluctuation of the temperature increased to ~10 °C. The measured temperature profile became significantly different each time the fiber end was replaced. Figures 2 and 3 show two typical temperature profiles analyzed with the Gabor and Fourier transforms, respectively. The temperature profiles were measured in a steady-state condition when the power of the argon-ion beam was ~3 W. The first temperature profile, shown in Figs. 2(a) and 3(a), indicates that the highest temperature is obtained at the input end of the fiber, probably due to defects caused by the cleavage operation. In previous research it has been shown that surface imperfections, such as dust, cleaning residues, impurities, and scratches, absorb and/or scatter light at a glass surface.[12] The maximum temperature increase in this case is ~3 times higher than the average temperature change along the whole grating, 26 °C. The temperature peak analyzed with the Fourier transform is narrower and has a higher amplitude than obtained with the Gabor transform, owing to the reduced spatial resolution in the Gabor transform. The full width at half-maximum of the Gaussian window used in the Gabor transform was 0.5 nm and therefore the spatial resolution was limited to 1.5 mm. Figures 2(b) and 3(b) show another typical temperature profile that was measured at the same power of the argon-ion laser that was used to obtain the results in Figs. 2(a) and 3(a). The temperature profile in this case is uniform and implies that the main heating cause is not the input surface of the fiber. The relatively low heating of the fiber might be caused by absorption of leaky modes and scattered waves generated by the coupling of the high-power beam and absorbed at the cladding surface. Hydrogen loading and grating fabrication might also affect absorption of the fiber. The attenuation of the optical fiber in the wavelength region of our argon-ion laser is ~15 dB/km, and therefore it should not cause significant heating of the fiber. The average temperature change in Fig. 2(b) equals 16 °C. This result is in accordance with the result from measuring the shift in the Bragg wavelength of the whole grating, 15 °C. The use of our measurement technique allows the temperature profile of the grating to be found rather than the average temperature of the whole grating. Therefore we could separate between heating effects caused at the input surface of the fiber, shown in Figs. 2(a) and 3(a) and heating effects caused at the input section of the fiber, shown in Figs. 2(b) and 3(b).

B. Temperature Profile in a Splice Region of Optical Fibers

We also studied changes in the temperature around a splice region of two optical fibers. The power of the argon-ion laser in the experiment was ~3 W and the coupling efficiency was ~40%. The location of the splice region could be measured by performing a Fourier analysis on the measured interference spectrum before turning on the high-power argon-ion laser.
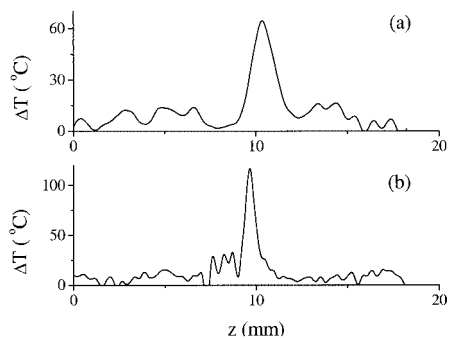
Fig. 4. Temperature distribution around the splice region of a multimode fiber analyzed by using (a) the Gabor transform and (b) the Fourier transform. The power of the argon-ion laser was 3 W, and the coupling efficiency was ~40%.

Strong phase distortion was observed in part of the impulse response that corresponds to the wave that was reflected from the splice region. Figures 4(a) and 4(b) show the measured temperature profile analyzed by using the Gabor and the Fourier transforms, respectively. Both Figs. 4(a) and 4(b) show a significant increase in the temperature around the splice region. The maximum temperatures measured by using Fourier analysis was ~125 °C. The temperature peak analyzed with the Fourier transform is narrower and has a higher amplitude than obtained with the Gabor transform, owing to the reduced spatial resolution in the Gabor transform. The strong heating might be caused by absorption at the outer interface of the cladding of leaky modes and scattered waves generated from the splice and by absorption of light by localized defects generated by the splicing process.

When the power of the argon-ion laser increased to more than 6 W for more than few minutes, we observed an irreversible erasure of the grating in the region of the fiber where high temperature was measured, as shown in Fig. 5. Figure 5 shows the absolute value of the normalized impulse response after erasure of part of the grating. The hole in the amplitude of the impulse response indicates that the grating was erased around the splice region. The
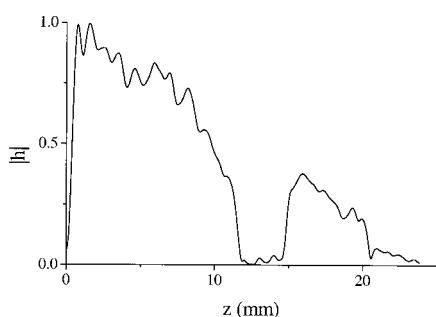
Fig. 5. Amplitude of the impulse response of a grating, written at a splice region of a fiber, measured after the power of the argon-ion laser was increased to 6 W for ~5 min. The hole in the amplitude of the impulse response indicates that the grating was erased around the splice region.

length of the part of the grating that was erased is ~3 mm. The erasure of the grating is another indication of the high temperatures generated in the splice region since a fast erasure of fiber gratings was observed in previous research only at very high temperatures (>200 °C).[13]

5. Conclusion

We have experimentally demonstrated a new method for measuring the change in the temperature distribution when a high-power laser beam is coupled into an optical fiber and when a high-power laser beam propagates through a splice region of two optical fibers. High-temperature changes have been measured. The measurement of the temperature profile rather than the average temperature along the grating enables the study of the cause of the fiber heating. The temperature measurement can be performed in real time without affecting the operation of the interrogated fiber system. The new measurement technique might be important for developing and improving the reliability of high-power fiber components.

References

1. V. Dominic, S. MacCormack, R. Waarts, S. Sanders, S. Bicknese, R. Dohle, E. Wolak, P. S. Yeh, and E. Zucker, "110 W fiber laser," Electron. Lett. **35,** 1158–1160 (1999).
2. D. C. Brown and H. J. Hoffman, "Thermal, stress, and thermo-optic effects in high average power double-clad silica fiber laser," IEEE J. Quantum Electron. **37,** 207–217 (2001).
3. A. D. Kersley, M. A. Davis, H. J. Patrick, M. LeBlanc, K. P. Koo, C. G. Askins, M. A. Putnam, and E. J. Friebele, "Fiber grating sensors," J. Lightwave Technol. **15,** 1442–1463 (1997).
4. S. Huang, M. M. Ohn, M. Leblanc, and R. M. Measures, "Continuous arbitrary strain profile measurements with fiber Bragg gratings," Smart Mater. Struct. **7,** 248–256 (1998).
5. S. Keren and M. Horowitz, "Interrogation of fiber gratings by use of low-coherence spectral interferometry of noiselike pulses," Opt. Lett. **26,** 328–330 (2001).
6. M. Horowitz, Y. Barad, and Y. Silberberg, "Noiselike pulses with a broadband spectrum generated from an erbium-doped fiber laser," Opt. Lett. **22,** 799–801 (1997).
7. M. A. Putnam, M. L. Dennis, I. N. Duling III, C. G. Askin, and E. J. Friebele, "Broadband square-pulses operation of passively mode-locked fiber laser for fiber Bragg grating interrogation," Opt. Lett. **23,** 138–140 (1998).
8. T. Erdogan, "Fiber grating spectra," J. Lightwave Technol. **15,** 1277–1294 (1997).
9. G. H. Song and S. Y. Shin, "Design of corrugated waveguide filters by the Gelfand–Levitan–Marchenko inverse-scattering method," J. Opt. Soc. Am. A **2,** 1905–1915 (1985).
10. H. Kogelnik, "Filter response of nonuniform almost-periodic structure," Bell Syst. Tech. J. **55,** 109–126 (1976).
11. D. Gabor, "Theory of communication," J. Inst. Elecr. Eng. **93** (III), 429–457 (1946).
12. M. Commandrè, P. Roche, J. P. Borgogno, and G. Albrand, "Absorption mapping for characterization of glass surfaces," Appl. Opt. **34,** 2372–2379 (1995).
13. T. Erdogan, V. Mizrahi, P. J. Lemaire, and D. Monroe, "Decay of ultraviolet-induced fiber Bragg gratings," J. Appl. Phys. **76,** 73–80 (1994).